ACS APPLIED MATERIALS & INTERFACES

Research Article

www.acsami.org

One-Pot Soft-Templating Method to Synthesize Crystalline Mesoporous Tantalum Oxide and Its Photocatalytic Activity for Overall Water Splitting

Limin Guo,*[,†] Hidehisa Hagiwara,[‡] Shintaro Ida,[‡] Takeshi Daio,[§] and Tatsumi Ishihara*[,†]

[†]International Institute for Carbon-Neutral Energy Research (WPI-I2CNER), [‡]Department of Applied Chemistry and [§]International Research Center for Hydrogen Energy, Kyushu University, 744 Motooka, Nishi-ku, Fukuoka 819-0395, Japan

Supporting Information

ABSTRACT: Crystalline mesoporous Ta_2O_5 has been successfully synthesized by a one-pot route using P-123 as the structure directing agent (SDA). A series of crystalline mesoporous Ta_2O_5 samples has been prepared by changing the calcination temperature. The surface area decreased and the pore size increased with the increasing calcination temperature, which were the results of crystallite growth. At the same time, the pore volume was well maintained, which means limited shrinkage during the calcination of elevated temperature. The porous structure and crystal structure of as-synthesized mesoporous Ta_2O_5 were characterized by XRD, TG-DTA, SEM, TEM, and N_2 sorption techniques. The photocatalytic activity of the as-synthesized mesoporous Ta_2O_5 with the cocatalyst NiO_x for overall water splitting under ultraviolet (UV) light irradiation was systematically evaluated. The photocatalytic activity of crystalline mesoporous Ta_2O_5 showed about 3 times that of commercial Ta_2O_5 powder and 22 times that of amorphous mesoporous Ta_2O_5.

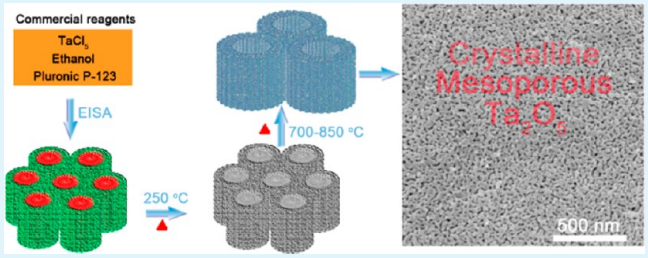

KEYWORDS: *soft-templating method, tantalum oxide (Ta_2O_5), crystalline, mesoporous, water splitting*

INTRODUCTION

Nowadays, global energy and environmental issues are very important topics for our human societies.[1,2] To construct clean or low-carbon energy systems or societies should be the inevitable trend, and hydrogen will play a key role due to its clean energy and successful utilization in fuel cells.[2] Solar water splitting may provide an economically viable procedure to the direct conversion of solar energy into renewable and storable hydrogen and oxygen, since both sunlight and water are abundant on our planet.[3] Approaches to solar water splitting include photocatalytic water splitting with homogeneous or heterogeneous photocatalysts, photoelectrochemical or photoelectrocatalytic water splitting, and electrolysis of water with photovoltaic cells coupled to electrocatalysts.[2,4−7] The heterogeneous photocatalytic water splitting is a very attractive reaction due to its simplicity and easily large-scale application.[2,7] The heterogeneous photocatalytic water splitting involves three major steps:[2,5] (i) adsorption of photons to generate electron-hole pairs; (ii) charge separation and migration to the surface of semiconductor; (iii) surface reactions for water reduction and oxidation. Photocatalytic water splitting can be realized when the above three sequential steps are completed. Subject to the three main steps, different methods have been developed to improve the final photocatalytic performance. For example, surveying narrow band gap semiconductor materials with proper levels of the conduction and valence bands (band engineering) to adsorb broad spectrum of solar energy and simultaneously achieve water splitting;[2] tune the physical properties of semiconductor materials, such as crystal structure, crystallinity, and particle size (materials engineering), in order to gain efficient charge separation and migration;[8] proper loading of cocatalysts (active sites) and increasing the surface area (more active sites).[9,10]

Due to their unique characteristics like high surface area, tunable pore size, and interconnected mesopores throughout the whole materials, crystalline mesoporous metal oxide synthesis and applications have attracted extensive attention.[11−16] The main metallic elements of metal oxide materials, which can be successfully applied as photocatalysts for water splitting, should have d^0 or d^{10} electronic configuration.[2,7] Considering high surface area (more cocatalysts and active sites) and thin crystalline wall (short distance for photoexcited electrons and holes to reach surface), the crystalline mesoporous d^0- and d^{10}-type metal oxides will be good candidates for photocatalytic water splitting. The higher photocatalytic performance of crystalline mesoporous metal oxides comparing with corresponding nonporous metal oxide is reasonable and expected. Notably, a high degree of crystallinity is quite important for water splitting because recombination between photogenerated electrons and holes is especially a

Received: August 8, 2013
Accepted: October 7, 2013
Published: October 7, 2013

serious problem for uphill water splitting reactions.[2] Up to now, there are a few papers reported on the crystalline mesoporous d^0 and d^{10} metal oxide synthesis. Wiesner's group[17] has successfully synthesized crystalline mesoporous TiO_2 and Nb_2O_5 using sp^2-hybridized-carbon containing polymer (poly(isoprene-block-ethylene oxide)) as the structure-directing agent. The special polymer was synthesized by themselves using an anionic polymerization method. There was no further photocatalytic water splitting data on the crystalline mesoporous TiO_2 and Nb_2O_5. Smarsly's group[18] reported the crystalline mesoporous $MgTa_2O_6$ thin films using special polymer KLE (poly(ethylene-*co*-butylne)-block-poly(ethylene oxide)), which also was synthesized by themselves using so-called "Kraton Liquid"[19] as the macroinitiator. For photocatalytic activity, only photodegradation experiment of Rhodamine B under UV-lamp has been carried out. It should be noted the photodegradation of organic dyes under UV light irradiation is quite different from the water splitting because the change in the Gibbs free energy for photodegradation of organic dyes is not so positive. For the synthesis of crystalline mesoporous Ta_2O_5, Domen's group[20] established a crystallization method using a silicone compound to form SiO_2 layers that strengthen the surface of amorphous Ta_2O_5 pore walls. After the high temperature crystallization, the silica was been removed by the concentrated NaOH solution. The photocatalytic water splitting under UV light irradiation of as-synthesized mesoporous Ta_2O_5 using NiO_x, RuO_2, or $Rh_{2-y}Cr_yO_3$ as cocatalyst demonstrated the crystalline mesoporous Ta_2O_5 was a very efficient photocatalyst. The photocatalytic activity of the NiO_x-loaded mesoporous Ta_2O_5 was improved to 7 times higher than that of the amorphous precursor by crystallization. Obviously, the synthesis of crystalline mesoporous Ta_2O_5 was quite important for final achievement of high photocatalytic performance. Up to now, the reported methods are still tedious, are high cost, have new impurity element introduction, or have high environmental impact. The simple and versatile method for crystalline mesoporous d^0- and d^{10}-typed metal oxides still needs to be further developed.

Herein, the one-pot synthesis method using the very common and commercial available polymer P-123 as the structure directing agent has been reported to synthesize crystalline mesoporous Ta_2O_5. The mesoporous Ta_2O_5 transformation from amorphous to crystal has been carefully investigated. Then, a series of crystalline mesoporous Ta_2O_5 with different surface area and pore size have been prepared. Finally, the photocatalytic water splitting activities of crystalline mesoporous Ta_2O_5 using NiO_x as cocatalyst were also systematically evaluated.

EXPERIMENTAL SECTION

Preparation of Crystalline Mesoporous Ta_2O_5. All reagents and solvents were commercially available and used without further purification or pretreatment. Briefly, 2.5 g of triblock copolymer P-123 ($HO(CH_2CH_2O)_{20}$-$(CH_2CH(CH_3)_{70}(CH_2CH_2O)_{20}H)$) was dissolved in 25 g of ethanol with constant stirring for 30 min. Then, 5.37 g of $TaCl_5$ was added into the solution under vigorous stirring. After another 1.5 h stirring, the sol solution was poured into Petri dishes for evaporation induced self-assembled process (EISA) at room temperature. After 1 week, a transparent gel was obtained. The gel was then treated at 250 °C for 12 h to partially decompose the polymer and condensate the Ta_2O_5 related species. Herein, the gel color was changed to black. After grinding, the sample powder was calcined at the elevated temperature for 30 min to completely remove the residual template and crystallize. The as-obtained samples were named as Ta_2O_5-500, Ta_2O_5-600, and so on for simplicity. The number 500 and 600 represent the calcination temperatures of 500 and 600 °C, respectively.

Characterization. Powder X-ray diffraction (XRD) patterns of tantalum oxides were recorded with a Rigaku X-ray diffractmeter/RINT2500HLR+ using Cu Kα radiation (40 kV and 80 mA). For small- and wide-angle XRD measurements, the scanning rates were 0.6 and 5°/min, respectively. Scanning electron microscopic (SEM) images were recorded with a Hitachi SU-8000 field emission electron microscope (FE-SEM). The powder samples were fixed on the carbon tape and directly used for observation. Transmission electron microscopic (TEM) images were taken by using a JEM-ARM200F apparatus with a spherical aberration corrector at an accelerating voltage of 200 kV. Samples for TEM observation were prepared by the following procedure: the as-synthesized mesoporous metal oxides powder were directly dispersed on a Cu grid. During the TEM observation, only the porous structure of a thin edge area of the small particles could be clearly observed due to the thickness or diameter of sample particles being too thick for the electron beam to penetrate. TG-DTA results were obtained with a Rigaku Thermo Plus TG8120 instrument with the air flow of 50 cm^3/min, and the heating rate was 10 °C/min. UV/vis diffuse reflectance spectra of the as-synthesized crystalline mesoporous Ta_2O_5 samples were measured using a spectrophotometer (Hitachi High-Technologies Co., Ltd., U-3310) with an attached integrating sphere. Nitrogen adsorption−desorption measurement were carried out at −196 °C with a BELSORP-MiniII (Bel Japan) instrument. Before measurements, samples were degassed at 150 °C for 8 h under N_2 flow. The specific surface area and the pore size distribution were calculated according to the Brunauer−Emmett−Teller (BET) and Barrett−Joyner−Halenda (BJH) models, respectively.

Photocatalytic Experimental Section. The photocatalytic water splitting was performed using a conventional closed circulating system. The catalyst (50 mg) was suspended in pure water (30 mL), which was presaturated with Ar. The 1 M KOH solution was used to adjust the pH to 11. A quartz reaction cell was irradiated by an external light source consisting of a 300 W Xe lamp (full arc). During photocatalytic water splitting, the suspension was mixed using a magnetic stirring bar. Ar gas (10.67 kPa) was used as the circulating carrier gas. Before the reaction started, the system was evacuated to remove the residual air and the absence of gas leakage was confirmed for 1 h by performing a reaction without light irradiation. The amounts of H_2 and O_2 formed were recorded and analyzed by gas chromatography with a thermal conductivity detector (Shimadzu Corp., GC-8A) through a gas sampler (around 10 cm^3 in volume), which was directly connected to the reaction system to avoid contamination from air. The light intensity of the Xe lamp was fixed around 0.25 W/cm^2 (the light intensity was measured by using a power meter (Ophir Optronics Ltd., 30A-P)) by adjusting the current value.

The NiO_x was used as the cocatalyst to promote the H_2 evolution and loaded onto Ta_2O_5 by an impregnation method.[20] $Ni(NO_3)_2 \cdot 6H_2O$ was used as the precursor to prepare aqueous solution. The certain volume $Ni(NO_3)_2$ solution was added into Ta_2O_5 powder and dried. The NiO loaded Ta_2O_5 was prepared by calcination at 300 °C for 1 h. Then, the NiO loaded Ta_2O_5 powder was treated under H_2 flow at 400 °C for 2 h. After that, the powder was softly oxidized under O_2 flow at 200 °C for 1 h to finally obtain NiO_x loaded Ta_2O_5 (the loading amount is calculated as NiO). The Pt was also used as cocatalyst for reference and loaded by evaporation to dryness using an aqueous solution of $[Pt(NH_3)_4(NO_3)_2]$, following the drying process on a hot-plate at 100 °C.[21]

RESULTS AND DISCUSSION

Preparation of Crystalline Mesoporous Ta_2O_5. Scheme 1 illustrates the proposed method to synthesize crystalline mesoporous Ta_2O_5. Notably, all the starting reagents were commercially available. The first step was the evaporation induced self-assembled process (EISA) to get homogeneous

Scheme 1. Schematic Illustration of the Proposed Method to Synthesize Crystalline Mesoporous Ta_2O_5[a]

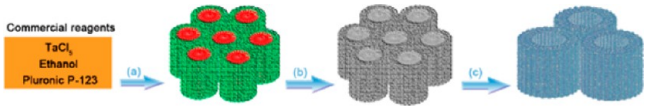

[a](a) EISA procedure to get homogeneous hybrid of P-123 and Ta species, (b) heat treatment at medium temperature to condensate Ta_2O_5 framework and simultaneously avoid the complete decomposition of P-123 template, and (c) high temperature calcination to complete removal of template and crystallization.

hybrid of P-123 and Ta species, which has already been reported by some references to synthesize amorphous mesoporous Ta_2O_5.[22,23] Thereafter, the obtained transparent gel was treated at 250 °C. During this stage, P-123 lost most of the O and H species, so the color of the gel after the heat treatment became black. In fact, amorphous mesoporous Ta_2O_5 has already formed after this step, although the Ta_2O_5 structure was still very loose, which would be analyzed and discussed later based on the TEM and N_2 sorption results. Finally, high temperature calcination has been carried out to completely remove the template and achieve the crystalline transformation of amorphous Ta_2O_5.

Figure 1 was the XRD patterns of as-synthesized mesoporous Ta_2O_5 and the commercial Ta_2O_5 powder for reference. From

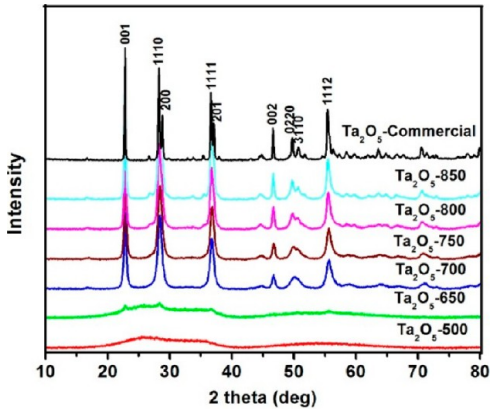

Figure 1. XRD patterns of Ta_2O_5 samples.

the 700 °C calcination on, clear diffraction peaks appeared and all the peaks can be ascribed to Ta_2O_5 (JCPDS No. 71-0639). The intensity of diffraction peaks gradually increased and narrowed with the increasing calcination temperature due to the crystallite size growth. The calculation by Scherrer's equation on the (001) diffraction peaks was used to estimate the crystallite size of as-synthesized crystalline mesoporous Ta_2O_5. The crystal size of Ta_2O_5-700, -750, -800 and -850 were 35, 39, 49, and 60 nm, respectively, and the trend was well consistent with the intensity increase of XRD diffraction peaks (Figure 1). The small-angle XRD patterns of mesoporous Ta_2O_5 samples (Figure S1, Supporting Information) showed one diffraction peak for Ta_2O_5-500 and Ta_2O_5-650, and the peak associated with wormlike mesoporous channels with uniform pore size. However, there was no similar diffraction peak for the Ta_2O_5-700, -750, -800, and -850 samples, which implied an obvious mesostructure change comparing with those of Ta_2O_5-500 and -650.

The N_2 sorption isotherms and pore size distribution of each sample in the preparation procedure were shown in Figure 2 and Figure S2 (Supporting Information), and physical properties obtained from XRD diffraction and N_2 sorption measurements are summarized in Table 1. All the N_2 sorption isotherms were the type-IV isotherm patterns, which were peculiar to mesoporous materials. For the amorphous mesoporous Ta_2O_5-250, -500, and -650, the pore size was estimated as 4.2 or 4.8 nm from N_2 uptake at $p/p_0 = 0.40-0.65$. The specific surface area and pore volume of Ta_2O_5-250 were 195.0 m^2/g and 0.22 cm^3/g, respectively, which were much higher than those of Ta_2O_5-500 and Ta_2O_5-650. From the N_2 sorption isotherm of Ta_2O_5-250 (Figure S2), an obvious uptake at low relative pressure can be observed, which associated with the existing of microporous structure. The low magnification TEM image of Ta_2O_5-250 (Figure S3a) showed obvious mesoporous structure and loose wall structure at the same time. Amorphous and microporous pore wall can be observed at high magnification TEM image (Figure S3b), which was consistent with the N_2 uptake at low relative pressure (Figure S2a). For the crystalline mesoporous Ta_2O_5 samples, the N_2 uptake leap gradually shifted to higher relative pressure with the calcination temperature increase (Figure 2a). The pore size of Ta_2O_5-700, -750, -800, and -850 centered 12.1, 16.0, 24.8, and 33.1 nm, respectively. The specific surface area of Ta_2O_5-700 was 41.3 m^2/g and decreased to 11.9 m^2/g for Ta_2O_5-850, which was the result of crystallite size growth. Notably, the total pore volume had no obvious change for all mesoporous Ta_2O_5 samples except Ta_2O_5-250, which demonstrated no obvious volume shrinkage accompanying with the crystallization transformation and crystallite growth. SEM images of crystalline mesoporous Ta_2O_5 samples are shown in Figure 3. Very clear mesoporous

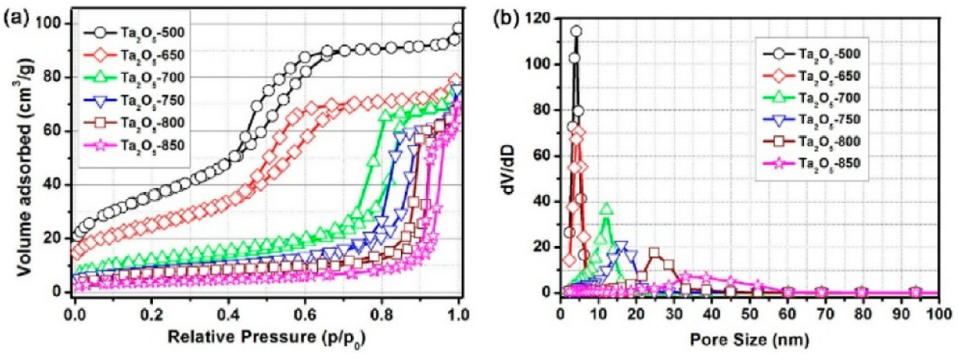

Figure 2. N_2 adsorption–desorption isotherms (a) and pore size distribution (b) of as-synthesized mesoporous Ta_2O_5 samples.

Table 1. Physical Properties of Ta_2O_5 Samples

sample name	$S_{BET}/m^2 \cdot g^{-1}$	pore size/nm	pore volume/mL·g^{-1}	crystallite size/nm
Ta_2O_5-commercial	2.3			114
Ta_2O_5-250	195.0	4.8	0.22	
Ta_2O_5-500	131.0	4.2	0.14	
Ta_2O_5-650	90.1	4.8	0.12	
Ta_2O_5-700	41.3	12.1	0.11	35
Ta_2O_5-750	28.4	16.0	0.10	39
Ta_2O_5-800	18.6	24.8	0.10	49
Ta_2O_5-850	11.9	33.1	0.10	60

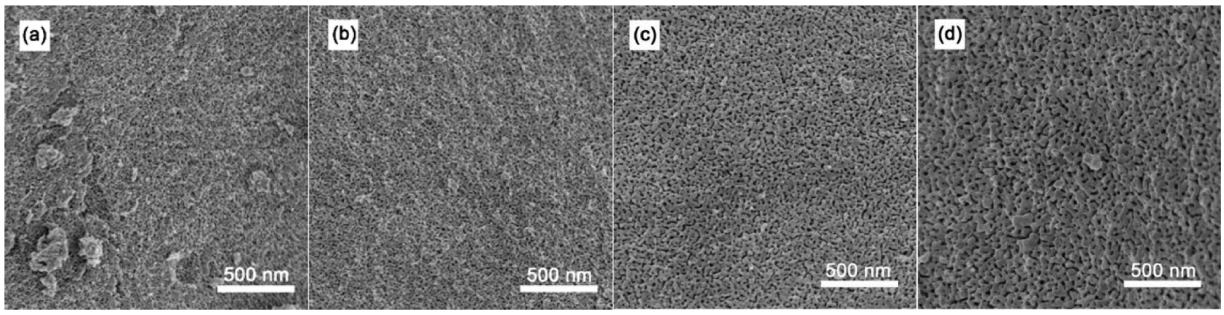

Figure 3. SEM images of crystalline mesoporous Ta_2O_5 samples: (a) Ta_2O_5-700, (b) Ta_2O_5-750, (c) Ta_2O_5-800, and (d) Ta_2O_5-850.

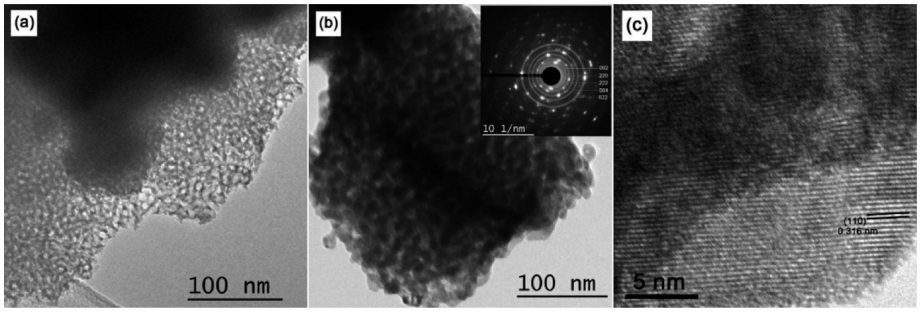

Figure 4. TEM images of amorphous mesoporous Ta_2O_5-500 (a), crystalline mesoporous Ta_2O_5-700 (selected area diffraction pattern (inset)) (b), and Ta_2O_5-700 with high resolution (c).

structure can be observed for all the samples. Furthermore, the pore size and wall thickness increased with the increase of calcination temperature, which was consistent with the results of XRD and N_2 sorption measurements. Figure 4a is the TEM image of Ta_2O_5-500. The clear mesoporous structure can be observed and the pore wall was compact comparing with that of Ta_2O_5-250 (Figure S2a). Figure 4b and c shows the low magnification TEM image, selected area diffraction pattern (inset), and high resolution TEM image of Ta_2O_5-700, which confirmed the walls were indeed crystalline. The final as-synthesized Ta_2O_5-700 was not the mixture of amorphous mesoporous Ta_2O_5 and crystalline Ta_2O_5. In addition, the mesopores were not the interspace of the isolated Ta_2O_5 nanoparticles. For the Ta_2O_5-750, -800, and -850, all the samples showed the characteristics of crystalline mesoporous Ta_2O_5 and the pore wall gradually became thicker with the increase of calcination temperature. The corresponding results are shown in Figure S4 (Ta_2O_5-750), Figure S5 (Ta_2O_5-800), and Figure S6 (Ta_2O_5-850). Figure 5 shows the TG-DTA curves of the sample Ta_2O_5-250, and the TG-DTA curves of P-123 and Ta_2O_5-EISA are enclosed in Figures S7 and S8, respectively. The first exothermal peak centered 439 °C (Figure 5) corresponds to the template decomposition accompanying around 17.4 wt % weight loss. The second exothermal peak

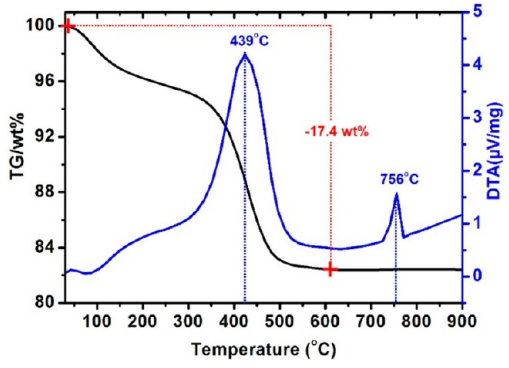

Figure 5. TG-DTA curves of the sample Ta_2O_5-250.

centered 756 °C corresponds to the transformation from amorphous to crystalline. However, the crystalline mesoporous Ta_2O_5 can be obtained at 700 °C calcination and the temperature was 56 °C lower than the value obtained by TG-DTA measurement. Maybe there were some other factors which influenced the kinetic process of Ta_2O_5 crystallization, and the detail for this was still not clear. In Figure S7, the exothermal peak centered 241 °C corresponds to the decomposition of P-123 accompanying with almost 100 wt %

weight loss. In Figure S8, the exothermal peak centered 313 °C also corresponds to the template decomposition accompanying with 52.1 wt % weight loss. From the results of TG-DTA measurements, the temperature corresponding to template decomposition shifted to much higher temperature for Ta_2O_5-250 compared with those of P-123 and Ta_2O_5-EISA, and the higher template decomposition temperature should be helpful to strengthen the pore structure before crystal transformation.

According to above characterizations and analysis, the crystalline mesoporous Ta_2O_5 has been successfully synthesized by proposed one-pot soft-templating method (Scheme 1). The final mesoporous Ta_2O_5 was not the mixture of amorphous mesoporous Ta_2O_5 and crystalline Ta_2O_5, and it should be the crystalline mesoporous Ta_2O_5. The mesoporous Ta_2O_5 has been already formed after the 250 °C heat treatment, although the pore wall structure was still loose and obvious microporous structure can be observed. Further increasing the calcination temperature to 500 °C, the condensation of porous Ta_2O_5 structure continued although the crystal transformation still did not happen, which was the reason that the surface area and pore volume decreased a lot for Ta_2O_5-500 comparing with those of Ta_2O_5-250. The mesopore size has no obvious change until the crystal transformation and there was a dramatic mesostucture change once the crystallization happened. The pore size and wall thickness increased with the calcination temperature increase, which associated with the crystallite growth of Ta_2O_5. Notably, the total pore volume had no obvious decrease, which implied the total structure can be well maintained. In addition, the proposed method here should be also applicable to synthesize other metal oxide and crystalline mesoporous Nb_2O_5 has been also successfully synthesized (Figure S9).

Photocatalytic Performance of As-Synthesized Crystalline Mesoporous Ta_2O_5. It was known NiO was a very good cocatalyst for many photocatalysts including Ta_2O_5.[24,25] The reduction and oxidation treatment of NiO into NiO_x (Ni metal particles covered with NiO) can further improve the photocatalytic performance of crystalline mesoporous Ta_2O_5.[20] The Ni metal particles made an ohmic contact between photocatalyst surface and NiO. Then, the photoexcited electrons can smoothly migrate to the NiO surface to reduce the water into H_2.[20,26] Herein, the dependence of the photocatalytic activity of as-synthesized crystalline mesoporous Ta_2O_5 on the loading amount of NiO_x (calculated as NiO) has been investigated (Figure 6 and Table S1). For the crystalline mesoporous Ta_2O_5, the activity significantly increased with the loading amount increase of NiO_x at first, and then gradually and slowly decreased. According to the photocatalytic data (Figure 6 and Table S1), the highest H_2 evolution rate for Ta_2O_5-700, Ta_2O_5-750, Ta_2O_5-800, and Ta_2O_5-850 were 1426.1, 1305.3, 1456.0, and 1180.3 $\mu mol \cdot g^{-1} \cdot h^{-1}$, respectively. Figure 7 gives the corresponding figures on the time course of gas evolution from water splitting. Stoichiometric O_2 evolution can also be observed. There were no significant decrease of H_2 and O_2 evolution rate within the 5h reaction, which implied negligible deactivation of corresponding photocatalysts. The photocatalytic activity depended on the experimental conditions, such as a light source and the type of the reaction cell, the activities cannot be compared with each other if the reaction conditions were different from each other.[2] Therefore, the photocatalytic activity of commercial crystalline Ta_2O_5 powder, Ta_2O_5-500, and Ta_2O_5-650 was also checked here for comparison and elucidation. Figure 1 and Supporting

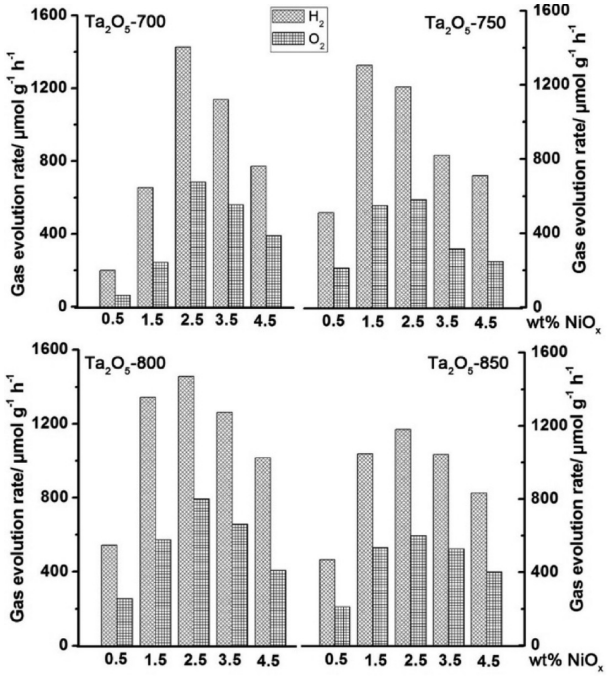

Figure 6. Dependence of the photocatalytic activity of as-synthesized crystalline mesoporous Ta_2O_5 on the loading amount of NiO_x.

Information Figure S10 show the XRD pattern and SEM image of Ta_2O_5-commercial, which demonstrates that the powder had good crystalline state and the size was several hundred nanometers. The surface area of Ta_2O_5-commercial powder was 2.3 m^2/g, which was much smaller than those of Ta_2O_5-500 and Ta_2O_5-600. However, the photocatalytic activity of Ta_2O_5-commercial-1.5 wt %NiO_x was much higher than those of amorphous Ta_2O_5-500-1.5 wt %NiO_x and Ta_2O_5-650-1.5 wt %NiO_x (Figure 8 and Table S1). For the crystalline mesoporous Ta_2O_5-700 and Ta_2O_5-800 after the optimal NiO_x loading amount (2.5 wt %), the photocatalytic activity was almost 3 times that of Ta_2O_5-commercial-1.5 wt %NiO_x. For the specific photocatalyts (the fixed crystal structure or band gap), the crystallinity, particle size, and surface area strongly affect the charge separation, migration of photogenerated carriers, and quantity of active sites. The higher the crystallinity is, the smaller the defects quantity is. The defects are trapping and recombination centers between photoexcited electrons and holes, which is a negative factor for photocatalytic activity. In general, crystallinity is increased with the elevated calcination temperature. If the pore wall becomes thin, the distance that photoexcited electrons and holes have to migrate to reaction sites on the surface becomes shorter and facilitates the carrier separation. In addition, the higher surface area means more loading amounts of effective co-catalysts and active sites. The final photocatalytic activity should be determined by the balance among these factors. Notably, a high degree of crytstallinity is often strictly required comparing with a high surface area for water splitting because recombination between photogenerated electrons and holes is a very serious problem for uphill reactions,[2] which should be the reason that Ta_2O_5-commercial has much higher activity than Ta_2O_5-500 and Ta_2O_5-650. Figure S10 shows the UV−vis diffuse reflectance spectra of as-synthesized mesoporous Ta_2O_5 and commercial Ta_2O_5. There was a blue shift for the absorption edge of Ta_2O_5-500, which may be due to the amorphous state of the sample.[27]

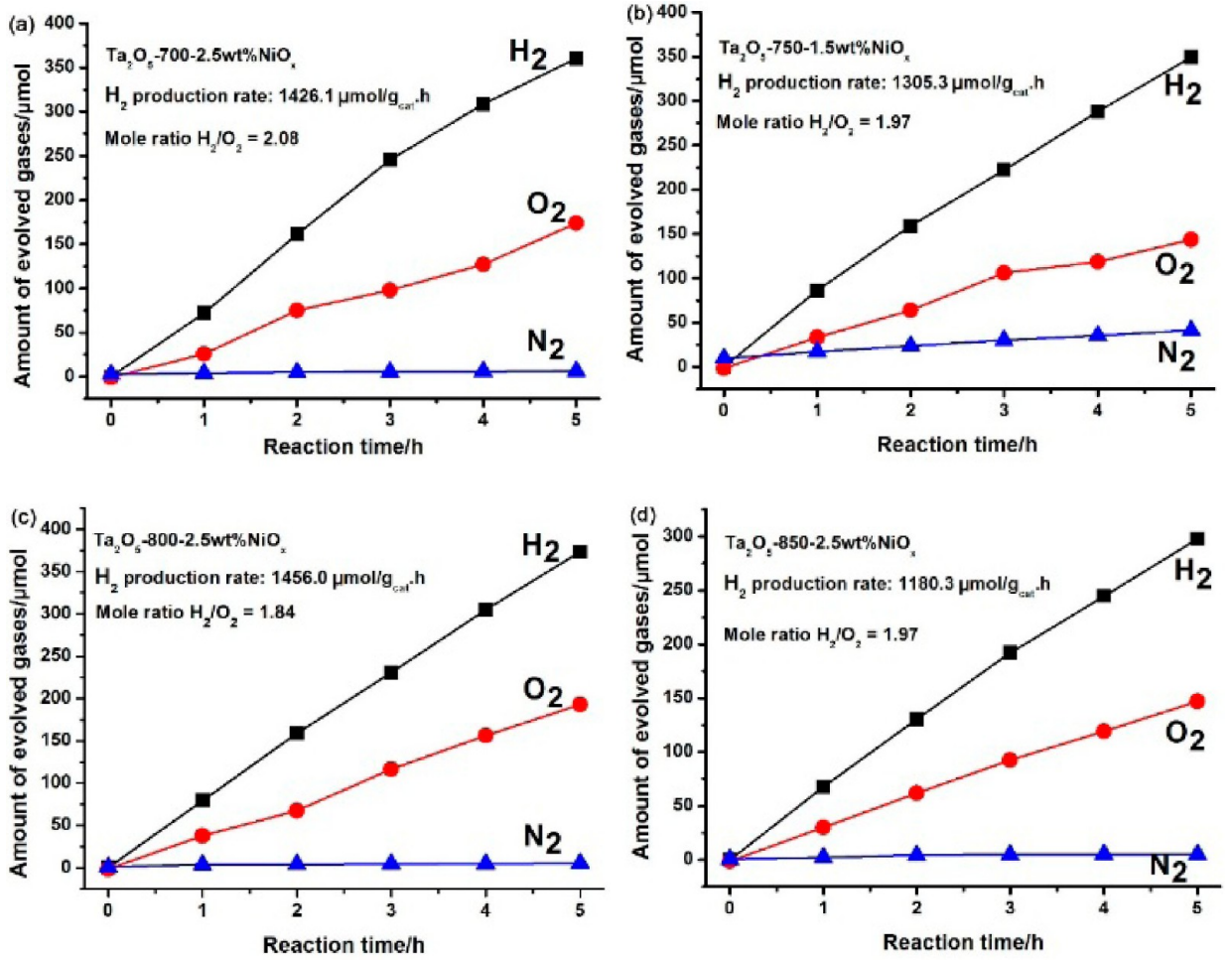

Figure 7. Time course of gas evolution from overall water splitting on (a) Ta_2O_5-700-2.5 wt %NiO_x, (b) Ta_2O_5-750-1.5 wt %NiO_x, (c) Ta_2O_5-800-2.5 wt %NiO_x, and (d) Ta_2O_5-850-2.5 wt %NiO_x. The N_2 amount was used to check the air leakage.

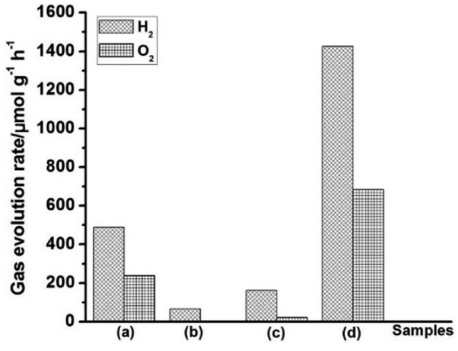

Figure 8. Photocatalytic activities of various Ta_2O_5 samples: (a) Ta_2O_5-commercial-1.5 wt %NiO_x, (b) Ta_2O_5-500-1.5 wt %NiO_x, (c) Ta_2O_5-650-1.5 wt %NiO_x, and (d) Ta_2O_5-700-2.5 wt %NiO_x.

For the crystalline mesoporous Ta_2O_5 samples, the absorption edge overlapped with that of Ta_2O_5-commercial. The adsorption near the adsorption edge (red circle in Figure S11) associated with the defects and gradually decreased with the calcination temperature increase, which implied the crystallinity increased with the elevated calcination temperature, and the spectrum of Ta_2O_5-850 overlapped with that of Ta_2O_5-commercial. On the other hand, the surface area of as-synthesized crystalline mesoporous Ta_2O_5 decreased with the elevated calcination temperature, which should be a negative factor for the corresponding photocatalytic activity. The final resultant photocatalytic activity of the crystalline mesoporous Ta_2O_5 was possibly determined by the two structural factor and did not monotonously decrease or increase. The structural characteristics of NiO_x loaded crystalline mesoporous Ta_2O_5 were also investigated. Figure S12 was the XRD patterns of Ta_2O_5-700, Ta_2O_5-700-4.5 wt %NiO_x, and just NiO_x. There were no obvious peaks related to NiO_x in the XRD pattern of Ta_2O_5-700-4.5 wt %NiO_x, which implied the size NiO_x particles should be nanosized. Figure 9 gives the high resolution TEM image of Ta_2O_5-700-4.5 wt %NiO_x and shows clear crystalline stripes, which can be well indexed as the (001) and (1110) of Ta_2O_5 and the (111) of Ni. The size of Ni particles was around 5 nm, which may elucidate the reason that no obvious diffraction peaks of Ni appeared in the corresponding XRD pattern (Figure S12). The Pt is also usually used as cocatalyst to promote H_2 evolution.[28,29] Here, the photocatalytic activity of the crystalline mesoporous Ta_2O_5-800-0.5 wt %Pt has also been checked and the photocatalytic activity was much lower than that of NiO_x loaded Ta_2O_5 samples and the O_2 evolution was not formed with a stoichiometric amount (Table S1), which may be due to serious back reaction between H_2 and O_2.

According to above experimental results and discussion, the NiO_x loaded crystalline mesoporous Ta_2O_5 samples showed much higher photocatalytic activity comparing with nonporous commercial Ta_2O_5 powder. In contrast, the NiO_x loaded

dx.doi.org/10.1021/am4032778 | ACS Appl. Mater. Interfaces 2013, 5, 11080−11086

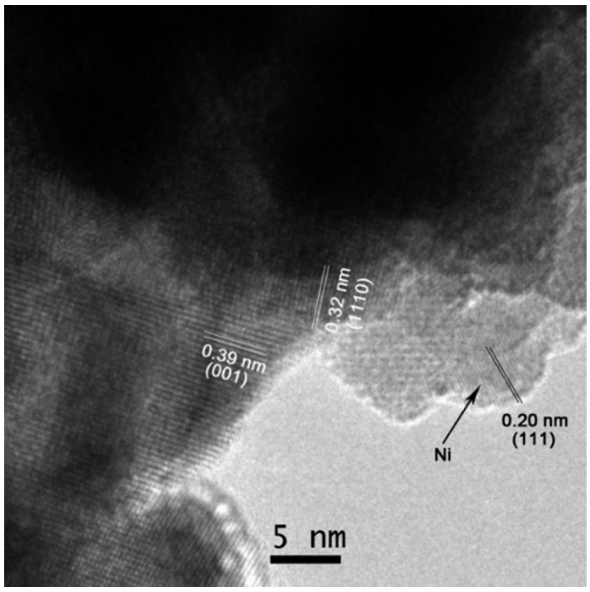

Figure 9. TEM image of Ta_2O_5-750-4.5 wt %NiO_x.

amorphous mesoporous Ta_2O_5 showed much lower photocatalytic activity, although it had very high surface area. Nevertheless, if the crystallinity can be well preserved, the mesoporous structure can further significantly improve the photocatalytic activity. Due to the wide band gap of Ta_2O_5 (4.0 eV), the water splitting can be only achieved under UV irradiation. Already there are some heterogeneous phtotocatlysts which can achieve water splitting under visible light irradiation, such as GaN:ZnO[30,31] and $SrTiO_3$:$BiVO_4$.[32] Further efforts to synthesize crystalline mesoporous photocatalysts with narrower band gap and proper conduction and valence bands for water splitting are on the way.

CONCLUSIONS

Crystalline mesoporous Ta_2O_5 has been successfully synthesized by a simple and one-pot soft-templating method using P-123 as SDA. The as-synthesized crystalline mesoporous Ta_2O_5 samples with NiO_x cocatalyst were efficient photocatalysts for overall water splitting under UV light irradiation, and the photocatalytic activity was about 3 times that of commercial Ta_2O_5 and 22 times that of amorphous mesoporous Ta_2O_5. Notably, both the crystalline pore wall and mesoporous structure of as-synthesized Ta_2O_5 samples contributed to the final enhanced photocatalytic activity. We believe the method offers a very convenient choice to synthesize crystalline mesoporous Ta_2O_5.

ASSOCIATED CONTENT

Supporting Information

XRD patterns, TG-DTA results, SEM images, TEM images, N_2 sorption isotherms, UV-Vis diffuse reflectance spectra, and photocatalytic data. This material is available free of charge via the Internet at http://pubs.acs.org.

AUTHOR INFORMATION

Corresponding Authors

*E-mail: lmguo1982@gmail.com (L.G.).
*E-mail: ishihara@cstf.kyushu-u.ac.jp (T. I.).

Notes

The authors declare no competing financial interest.

ACKNOWLEDGMENTS

This work was supported by the International Institute for Carbon-Neutral Energy Research (WPI-I^{2}CNER), which was established by the World Premier International Research Center Initiative (WPI), MEXT, Japan.

REFERENCES

(1) Lewis, N. S.; Nocera, D. G. *Proc. Natl. Acad. Sci. U.S.A.* **2006**, *103*, 15729−15735.
(2) Kudo, A.; Miseki, Y. *Chem. Soc. Rev.* **2009**, *38*, 253−278.
(3) Ma, S. S. K.; Hisatomi, T.; Maeda, K.; Moriya, Y.; Domen, K. *J. Am. Chem. Soc.* **2012**, *134*, 19993−19996.
(4) Youngblood, W. J.; Lee, S. A.; Maeda, K.; Mallouk, T. E. *Acc. Chem. Res.* **2009**, *42*, 1966−1973.
(5) Yang, J. H.; Wang, D. E.; Han, H. X.; Li, C. *Acc. Chem. Res.* **2013**, *46*, 1900−1909.
(6) Walter, M. G.; Warren, E. L.; Mckone, J. R.; Boettcher, S. W.; Mi, Q. X.; Santori, E. A.; Lewis, N. S. *Chem. Rev.* **2010**, *110*, 6446−6473.
(7) Maeda, K.; Domen, K. *J. Phys. Chem. Lett.* **2010**, *1*, 2655−2661.
(8) Tong, H.; Ouyang, S. X.; Bi, Y.P.; Umezawa, N.; Oshikiri, M.; Ye, J. H. *Adv. Mater.* **2012**, *24*, 229−251.
(9) Li, R. G.; Zhang, F. X.; Wang, D. E.; Yang, J. X.; Li, M. R.; Zhu, J.; Zhou, X.; Han, H. X.; Li, C. *Nat. Commun.* **2013**, *4*, 1432.
(10) Takahara, Y.; Kondo, J. N.; Takata, T.; Lu, D. L.; Domen, K. *Chem. Mater.* **2001**, *13*, 1194−1199.
(11) Schüth, F. *Chem. Mater.* **2001**, *13*, 3184−3195.
(12) Ren, Y.; Ma, Z.; Bruce, P. G. *Chem. Soc. Rev.* **2012**, *41*, 4909−4927.
(13) Yue, W. B.; Zhou, W. Z. *Prog. Nat. Sci.* **2008**, *18*, 1329−1338.
(14) Kondo, J. N.; Domen, K. *Chem. Mater.* **2008**, *20*, 835−847.
(15) Shi, J. L. *Chem. Rev.* **2013**, *113*, 2139−2181.
(16) Zhang, R. Y.; ElZatahry, A. A.; Al-Deyab, S. S.; Zhao, D. Y. *Nano Today* **2012**, *7*, 344−366.
(17) Lee, J. W.; Orilall, M. C.; Warren, S. C.; Kamperman, M.; Disalvo, F. J.; Wiesner, U. *Nat. Mater.* **2008**, *7*, 222−228.
(18) Wu, J. M.; Djerdj, I.; Graberg, T. V.; Smarsly, B. M. *Beilstein J. Nanotechnol.* **2012**, *3*, 123−133.
(19) Bresesinski, T.; Wang, J.; Tolbert, S.; Dunn, B. *Nat. Mater.* **2010**, *9*, 145−151.
(20) Noda, Y.; Lee, B.; Domen, K.; Kondo, J. N. *Chem. Mater.* **2008**, *20*, 5361−5367.
(21) Hagiwara, H.; Inoue, T.; Kaneko, K.; Ishihara, T. *Chem.—Eur. J.* **2009**, *15*, 12862−12870.
(22) Yang, P. D.; Zhao, D. Y.; Margolese, D. I.; Chmelka, B. F.; Stucky, G. D. *Nature* **1998**, *396*, 152−155.
(23) Nakajima, K.; Hara, M.; Domen, K.; Kondo, J. N. *Chem. Lett.* **2005**, *34*, 394−395.
(24) Takata, T.; Rurumi, Y.; Shinohara, K.; Tanaka, A.; Hara, M.; Kondo, J. N.; Domen, K. *Chem. Mater.* **1997**, *9*, 1063−1064.
(25) Takata, T.; Tanaka, A.; Hara, M.; Kondo, J. N.; Domen, K. *Catal. Today* **1998**, *44*, 17−26.
(26) Domen, K.; Kudo, A.; Onishi, T.; Kosugi, N.; Kuroda, H. *J. Phys. Chem.* **1986**, *90*, 292−295.
(27) Ohtani, B. *Chem. Lett.* **2008**, *37*, 217−229.
(28) Sayama, K.; Arakawa, H. *J. Chem. Soc., Faraday Trans.* **1997**, *93*, 1647−1654.
(29) Hagiwara, H.; Ono, N.; Inoue, T.; Matsumoto, H.; Ishihara, T. *Angew. Chem., Int. Ed.* **2006**, *45*, 1420−1422.
(30) Maeda, K.; Takata, T.; Hara, M.; Saito, N.; Inoue, Y.; Kobayashi, H.; Domen, K. *J. Am. Soc. Chem.* **2005**, *127*, 8286−8287.
(31) Maeda, K.; Teramura, K.; Lu, D.L.; Takata, T.; Saito, N.; Inoue, Y.; Domen, K. *Nature* **2006**, *440*, 295−295.
(32) Kato, H.; Hori, M.; Konta, R.; Shimodaira, Y.; Kudo, A. *Chem. Lett.* **2004**, *33*, 1348−1349.